

Theoretical study of mutual neutralization in $\text{He}^+ + \text{H}^-$ collisions

Åsa Larson,^{1,*} Sifiso M. Nkambule,¹ and Ann E. Orel²

¹*Department of Physics, Stockholm University, AlbaNova University Center, SE-106 91 Stockholm, Sweden*

²*Department of Chemical Engineering, University of California, Davis, California 95616, USA*

(Received 7 June 2016; published 17 August 2016)

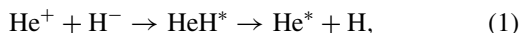
Total and differential cross sections for mutual neutralization in He^+ and H^- collisions at low to intermediate (0.001 eV to 100 eV) are calculated *ab initio* and fully quantum mechanically. Atomic final-state distributions and isotope effects are investigated. The theoretical model includes dynamics on eleven coupled states of $^2\Sigma^+$ symmetry, where autoionization is incorporated. The potential-energy curves, autoionization widths, and nonadiabatic couplings of electronic resonant states of HeH are computed by combining structure calculations with electron scattering calculations. The nuclear dynamics is studied using a strict diabatic representation of the resonant states. Effects of rotational couplings between $^2\Sigma^+$ and $^2\Pi$ electronic states are investigated in the pure precession approximation.

DOI: [10.1103/PhysRevA.94.022709](https://doi.org/10.1103/PhysRevA.94.022709)

I. INTRODUCTION

In mutual neutralization, oppositely charged ions collide and, driven by nonadiabatic couplings, an electron is transferred resulting in formation of neutral fragments. An *ab initio* description of the reaction is challenging since dynamics on highly excited electronic states has to be considered and the reaction is induced by nonadiabatic couplings between ionic and covalent states, often occurring at large internuclear distances. In the past there have been numerous semiclassical studies [1–3] of the process using, e.g., the Landau-Zener model [4,5] or similar approaches. Currently, there are just a handful of fully quantum mechanical *ab initio* studies of the MN reaction and all are limited to collisions between atomic ions [6–14].

Here, mutual neutralization in collisions of He^+ with H^- is theoretically studied, i.e.,



where the asterisk denotes electronic excitation. The calculation is performed *ab initio* and fully quantum mechanically. Potential-energy curves and nonadiabatic interactions are computed using the configuration-interaction method. The electronic states of the HeH complex formed in the reaction are autoionizing states (they are electronic resonant states) since they have potential energies larger than the energy of the ground state of HeH^+ . The present model includes autoionization using local complex potentials. With the complex-Kohn variational method [15], fixed nuclei electron-scattering calculations are carried out and the autoionization widths are computed. The adiabatic resonant states are diabaticized and the nuclear dynamics are studied using Johnson's log-derivative method [16,17].

The $\text{He}^+ + \text{H}^-$ mutual neutralization reaction is an ideal reaction for testing theory. The reaction forms a molecular complex simple enough for accurate quantum chemistry and electron-scattering calculations. However, the reaction is also challenging to theoretically describe since it involves very

highly excited electronic states that couple to the ionization continuum. To accurately describe the process, a manifold of avoided crossings occurring at internuclear distances ranging from $7a_0$ to $37a_0$ must be considered.

Using crossed and merged beam experiments, the cross section for mutual neutralization in collisions of $^4\text{He}^+$ with H^- has been measured, for energies ranging from a few eV to several keV [18–22]. Additionally, measurements on the cross section for mutual neutralization in $^4\text{He}^+ + \text{D}^-$ collisions have been performed [2,22].

The $\text{He}^+ + \text{H}^-$ mutual neutralization reaction was first theoretically studied using the semiclassical Landau-Zener model including ten coupled states [2]. It was found that the cross section depends on the ionic-covalent coupling parameters used in the model. By applying coupling elements developed by Olson *et al.* [2], good agreement with measured cross section below 2 keV was obtained. In 1992, Ermolaev [23] calculated the neutralization cross section at higher collision energies using a one-active-electron model. In the theoretical study by Chibisov *et al.* [24], all three electrons were included. The nuclear motion was described classically and autoionization was not considered. The total cross section as well as the final-state distributions were calculated for collision energies ranging between 40 to 4000 eV.

The present study presents a theoretical *ab initio* investigation of the mutual neutralization reaction where all degrees of freedom are described quantum mechanically and autoionization is incorporated. Section II describes how the relevant potential-energy curves and autoionization widths of the resonant states are obtained by combining electron-scattering and structure calculations. Additionally, the nonadiabatic couplings driving the reaction are computed. We also formulate the coupled nuclear Schrödinger equation for the resonant states and describe the diabaticization procedure and how the resulting coupled equation is solved using the log-derivative method. In Sec. III, we present not only the total neutralization cross section, but also the final-state distributions, differential cross section as well as an analysis of the effect of isotopic substitution. Unless otherwise mentioned, atomic units are used.

*aasal@fysik.su.se

II. THEORY

A. Electronic-structure and scattering calculations

In Fig. 1, the potential-energy curves of the HeH^+ and HeH systems are shown. The $X^1\Sigma^+$ electronic ground state of HeH^+ has the dominant configuration $(1\sigma)^2$. This state is associated with the $\text{He} + \text{H}^+$ fragments at large internuclear distances. The two lowest excited electronic states of the ion are the $a^3\Sigma^+$ and $A^1\Sigma^+$ states with dominant configurations corresponding to triplet and singlet coupled $(1\sigma)^1(2\sigma)^1$, respectively. These states have repulsive potential-energy curves dissociating into $\text{He}^+ + \text{H}$. The $X^2\Sigma^+$ electronic ground state of HeH has a repulsive potential. Below the potential of the ground state of HeH^+ , there are manifolds of Rydberg states with potential-energy curves similar to the ground state of the ion. These are displayed with thin blue dashed curves in Fig. 1. There are also Rydberg states converging to the excited ionic cores. These states have potential-energy curves situated in the ionization continuum of the ground ionic state and through electronic interactions, they will interact with the continuum and hence they are electronic resonant states. These states dissociate into $\text{He}^* + \text{H}$ and are illustrated with thin solid black curves in Fig. 1. The ion-pair fragments $\text{He}^+ + \text{H}^-$ form a molecular state of $^2\Sigma^+$ symmetry. At large internuclear distances the potential of the ion-pair state is described by an attractive Coulomb potential and it will cross many of the covalent resonant states dissociating into $\text{He}^* + \text{H}$.

The present study includes eleven electronic resonant states of HeH of $^2\Sigma^+$ symmetry. These are the electronic states associated with $\text{He}[(1s)^1(nl)^1] + \text{H}[(1s)^1]$ limits, where $n = 2$ and $n = 3$. The $n = 4$ states are energetically below the ion-pair limit, but the avoided crossing distances induced by the ionic-covalent interactions are anticipated to be larger than $100a_0$ and these states are therefore neglected [7].

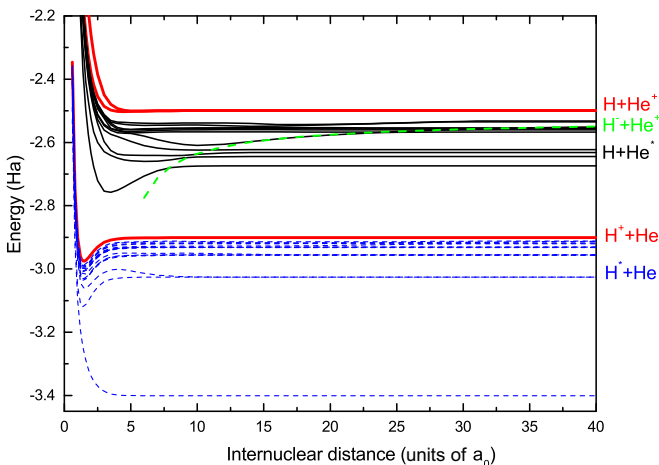


FIG. 1. Potential-energy curves of the HeH^+ and HeH systems. The potential-energy curves of the ground and first two excited states of HeH^+ are displayed with thick red curves. The potential-energy curves of the Rydberg states of HeH converging to the ground ionic core are shown with thin dashed blue curves, while thin black curves are the electronic resonant states. The dashed green curve illustrates the quasidiabatic Coulomb potential of the ion-pair state.

The electronic-scattering and structure calculations are carried out using the MESA program [25]. To calculate potential-energy curves of the HeH^+ and HeH systems, the full configuration-interaction (FCI) method is used with the aug-cc-pVQZ basis set for He [26] and the aug-cc-pVTZ basis set for H [27]. Extra diffuse functions are added on He to accurately describe the $3d$ orbitals.

The electron-scattering calculations cannot be carried out at the full-CI level. Instead by employing the complex-Kohn variational method [15], the same basis is used to construct natural orbitals of the ground state of HeH at the full-CI level. This is followed by a multireference configuration-interaction (MRCI) calculation, where the reference configurations are obtained by allowing for excitations of the three electrons among ten natural orbitals. Single external excitations are then added. By minimizing the complex-Kohn functional [15], unknown parameters of the scattering trial wave function can be optimized. This allows for determination of the scattering matrix and the corresponding eigenphase sum. We then extract fixed nuclei energy positions and autoionization widths of the resonant state by fitting the eigenphase sum to a Breit-Wigner form [28].

The radial first-derivative nonadiabatic coupling elements, $f_{ij}(R) = \langle \Phi_i | \frac{\partial}{\partial R} | \Phi_j \rangle$, are calculated analytically [29] using the MESA program. These calculations cannot be performed at the FCI level. Instead, using the same basis set, the multiconfiguration self-consistent field (MCSCF) method is used with an active space including all three electrons and ten orbitals. This is followed by a MRCI calculation where the reference configurations are generated by allowing for excitations of the three electrons among ten orbitals. Up to double external excitations are then included. These calculations are carried out in no symmetry. The resonant states are identified by analyzing the dominant configurations of the CI wave function. Since the sign of the electronic wave function is arbitrary, there are ambiguities in the signs of the coupling elements. The signs of these couplings are determined by an optimization procedure where all signs of the electronic wave functions are optimized such that the difference between the sum of all coupling elements with previous calculated point is minimized.

It should be noted that at small internuclear distances ($R < 5a_0$), the autoionization widths of the resonant states are nonzero. This is the region where these states become resonant states and will couple to the ionization continuum. When the nonadiabatic coupling elements are computed, the continuum part of the wave function of the resonant states is not included. The resonant states are treated as bound states and this is an approximation. To accurately compute nonadiabatic couplings among electronic resonant states is an interesting and challenging project beyond the goal of the present work. Additionally, as will be seen below, the nonadiabatic couplings among the resonant states occurring at small internuclear distances are not significant for the mutual neutralization reaction studied here.

To confirm the nonadiabatic couplings, they have also been computed at the full CI level using a three-point finite difference method with a step size of $0.1a_0$. In our FCI calculation, we use molecular orbitals that were optimized for $R = 40.0a_0$. Therefore, the atomic orbital coefficients are R independent, and we assume all derivatives in the

electronic wave functions originate from derivatives in the CI coefficients. The nonadiabatic coupling elements computed using finite difference and the analytical method are similar in magnitude and shape.

B. Nuclear Schrödinger equation for the resonant states

Following the P- and Q-projection operator formalism [30,31] an equation for the nuclear motions on the resonant states can be derived. These *adiabatic* resonant states are still interacting to each other by nonadiabatic interactions and by applying a partial wave expansion of the nuclear wave function, the radial Schrödinger equation for the dynamics on the resonant states can be derived. For fixed angular momentum ℓ , the equation is given by

$$\left[-\frac{1}{2\mu} \frac{d^2}{dR^2} + V_i + \frac{\ell(\ell+1)}{2\mu R^2} \right] u_{i,\ell} + \sum_j \left[W_{ij} - \frac{1}{\mu} f_{ij} \frac{d}{dR} - \frac{1}{2\mu} g_{ij} \right] u_{j,\ell} = E u_{i,\ell}. \quad (2)$$

Here, the electronic states are approximate eigenstates of the electronic Hamiltonian $\langle \Phi_i | \hat{H}_{el} | \Phi_j \rangle = V_i(R) \delta_{ij}$ coupled by the nonadiabatic coupling elements $f_{ij}(R) = \langle \Phi_i | \frac{\partial}{\partial R} | \Phi_j \rangle$ and $g_{ij}(R) = \langle \Phi_i | \frac{\partial^2}{\partial R^2} | \Phi_j \rangle$. Autoionization is included through the complex matrix elements W_{ij} . For electronic resonant states with high enough energy, the “*local Boomerang approximation*” [32,33] is justified, where autoionization into a complete set of vibrational eigenstates is assumed. We neglect the energy shift of the resonant states and the W_{ij} elements become purely imaginary of the form [31,34]

$$W_{ij}(R) = -i \frac{\sqrt{\Gamma_i(R)\Gamma_j(R)}}{2}. \quad (3)$$

The diagonal elements $W_{ii} = -i\Gamma_i/2$ account for the autoionization, while the off-diagonal elements cause indirect electronic couplings between the resonant states through the ionization continuum. By combining the electronic structure with the electron-scattering calculations described above, the potential energies of the adiabatic resonant states $V_i(R)$, nonadiabatic coupling elements $f_{ij}(R)$, and autoionization widths $\Gamma_i(R)$ are computed.

C. Diabatization

We assume that a finite number (11 in the present study) adiabatic electronic HeH states of $^2\Sigma^+$ symmetry are coupled by nonadiabatic couplings. By applying an orthogonal transformation, the adiabatic states may be transformed to a “*strict diabatic*” representation [35]. The transformation matrix, \mathbf{T} , can be obtained by integrating the equation

$$\left(\mathbf{1} \frac{d}{dR} + \mathbf{f} \right) \mathbf{T} = \mathbf{0}. \quad (4)$$

Here \mathbf{f} is an antisymmetric matrix containing the first-derivative nonadiabatic coupling elements. The boundary condition of the transformation matrix is given by the unit matrix at large internuclear distances. We thus assume that

asymptotically, the adiabatic and diabatic states are identical and any nonzero asymptotic nonadiabatic couplings are hence neglected. Once the transformation matrix is computed, we transform the adiabatic nuclear Schrödinger equation (2) to the corresponding diabatic one

$$\left[-\frac{1}{2\mu} \frac{d^2}{dR^2} + \frac{\ell(\ell+1)}{2\mu R^2} \right] \tilde{u}_{i,\ell} + \sum_j [\tilde{V}_{ij} + \tilde{W}_{ij}] \tilde{u}_{j,\ell} = E \tilde{u}_{i,\ell}, \quad (5)$$

where $\tilde{\mathbf{V}} = \mathbf{T}^T \mathbf{V} \mathbf{T}$ and $\tilde{\mathbf{W}} = \mathbf{T}^T \mathbf{W} \mathbf{T}$.

D. Log-derivative method

Instead of directly solving the coupled nuclear Schrödinger equation (5) in the diabatic representation, the logarithmic derivative of the radial wave function ($\mathbf{y}_\ell = \tilde{\mathbf{u}}'_\ell \tilde{\mathbf{u}}_\ell^{-1}$) is introduced and the radial Schrödinger equation is transformed to a matrix Riccati equation. The physical boundary condition for the logarithmic derivative at origin becomes a diagonal matrix with very large (approximately infinite) diagonal elements. Using a numerical procedure developed by Johnson [16,17,36], the matrix Riccati equation is integrated out to a distance (R_f) where the potentials have reached their asymptotic form. In the present study $R_f = 50a_0$ is used.

By combining the asymptotic value of logarithmic derivative with the correct regular and irregular solutions of the asymptotic states, the reactance matrix can be calculated [10]. The elements of the scattering matrix [$S_{ij,\ell}(E)$] are obtained as a Cayley transformation between the open partitions of the reactance matrix. Finally, the cross section for mutual neutralization can be computed from the scattering matrix elements

$$\sigma_{ij}(E) = \frac{\pi}{k_j^2} \sum_{\ell=0}^{\infty} (2\ell+1) |S_{ij,\ell} - \delta_{ij}|^2, \quad (6)$$

where $k_j = \sqrt{2\mu(E - E_j^{th})}$ is the asymptotic wave number of the incoming channel and E_j^{th} is the asymptotic energy of state j . The summation of partial waves is terminated when the ratios of partial cross section to accumulated total cross section are less than 10^{-4} for 25 terms in succession. The total neutralization cross section is obtained by summarizing the contributions from all covalent states.

By calculating the scattering amplitude

$$f_{ij}(\theta, E) = \frac{1}{2i\sqrt{k_i k_j}} \sum_{\ell=0}^{\infty} (2\ell+1) (S_{ij,\ell} - \delta_{ij}) P_\ell(\cos\theta), \quad (7)$$

where P_ℓ are the Legendre polynomials, the differential cross section is obtained from

$$\frac{d\sigma_{ij}}{d\Omega} = \frac{k_i}{k_j} |f_{ij}(\theta, E)|^2. \quad (8)$$

The formalism outlined above are usually applied to study nuclear dynamics on electronically bound states. However, the method can also be used to calculate cross section when autoionization is added to the model using local complex potentials [11,37,38].

III. RESULTS AND DISCUSSION

We start by presenting the potential-energy curves, autoionization widths, and nonadiabatic coupling elements important for the description of the $\text{He}^+ + \text{H}^-$ mutual neutralization reaction. This is followed by an analysis of the total neutralization cross section, where we investigate the role of the autoionization widths and rotational couplings. The reaction is studied for collisions of various hydrogen and helium isotopes. Finally, the final-state distributions and differential cross sections are presented.

A. Molecular data of the resonant states

Potential-energy curves of electronic resonant HeH states are computed using the FCI method described above. At the same level of theory, the lowest three electronic states of the cation are also computed. As can be seen in Fig. 2, the potential-energy curves of the resonant states have energies larger than the ground-state energy of the ion. In the figure, we show potential-energy curves of 11 resonant states of $^2\Sigma^+$ symmetry and 6 $^2\Pi$ resonant states. We also obtain the resonance positions from the electron-scattering calculations carried out with the MRCI method. These scattering calculations are carried out for internuclear distances smaller than $5.0a_0$. As can be seen in Fig. 2, the energy positions obtained using the FCI structure and MRCI scattering calculations agree well.

From the electron-scattering calculations not only the energy positions of the resonant states are obtained, but also the corresponding autoionization widths displayed in Fig. 3 for resonant states of $^2\Sigma^+$ symmetry. The two lowest resonant states have the largest widths. All widths become negligible at internuclear distances larger than $5.0a_0$.

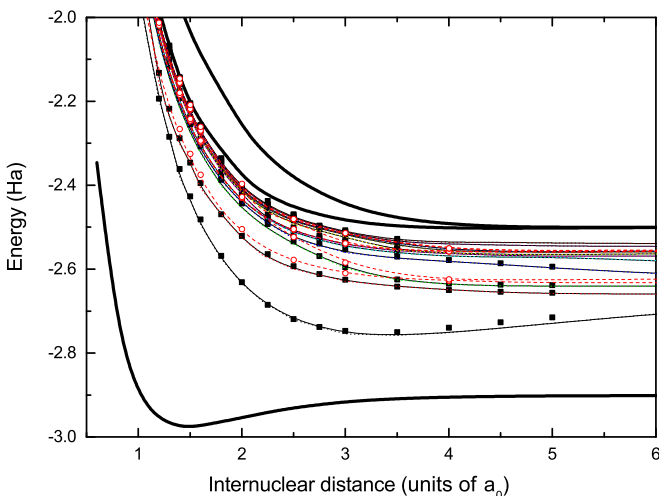


FIG. 2. Potential-energy curves of the $^2\Sigma^+$ (thin solid black lines) and $^2\Pi$ (thin dashed red lines) electronic resonant states of HeH are displayed together with the three lowest potential-energy curves of HeH^+ (thick black lines). The curves show the potential energies obtained with FCI structure calculations, while the (filled or open) symbols mark the corresponding energies obtained using electron scattering calculations at the MRCI level for resonant states of $^2\Sigma^+$ and $^2\Pi$ symmetries.

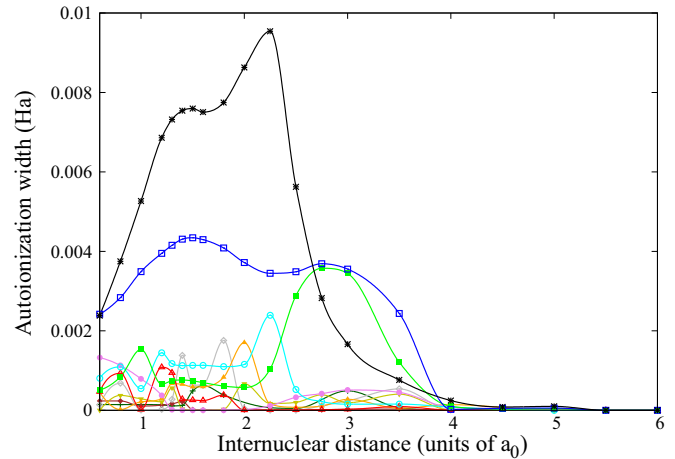


FIG. 3. Autoionization widths of the $^2\Sigma^+$ electronic resonant states of HeH obtained using electron-scattering calculations at fixed internuclear distances.

Figure 4 shows the potential-energy curves of the electronic resonant states of $^2\Sigma^+$ symmetry. At large internuclear distances there are avoided crossings occurring due to the interactions between the ion-pair and covalent states. For distances larger than $20a_0$, there are sharp avoided crossings among the ion-pair state and the covalent states associated with $\text{He}[(1s)^1(nl)^1] + \text{H}$ limits, where $n = 3$, as shown in Fig. 5(a). As will be seen, nonadiabatic first-derivative coupling elements $f_{ij}(R)$ among these states are the interactions driving the $\text{He}^+ + \text{H}^-$ mutual neutralization reaction. These couplings are displayed in Fig. 5(b). The nonadiabatic coupling elements are large in the vicinity of the avoided crossings and they have approximately Lorentzian profiles. The large coupling at $26a_0$ is not originating from an interaction between ionic and covalent states, but is due to an avoided crossing between states 9 and 10.

In Fig. 6, the coupling elements between all neighboring states are displayed for internuclear distances ranging from 0.5 to $6a_0$ in (a) and from 6 to $15a_0$ in (b). For internuclear

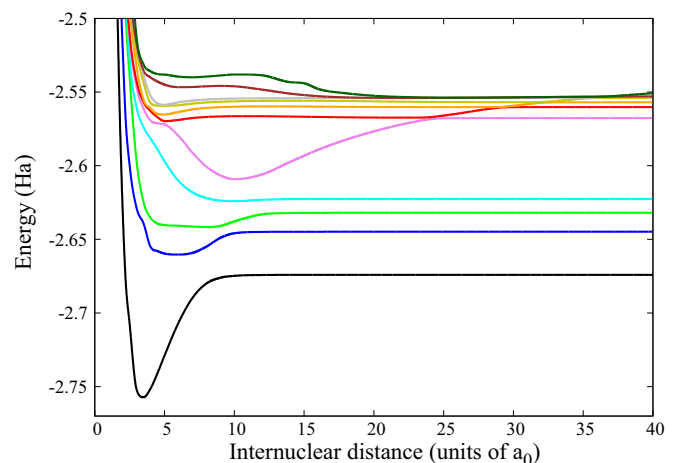


FIG. 4. Potential-energy curves of $^2\Sigma^+$ electronic resonant states of HeH.

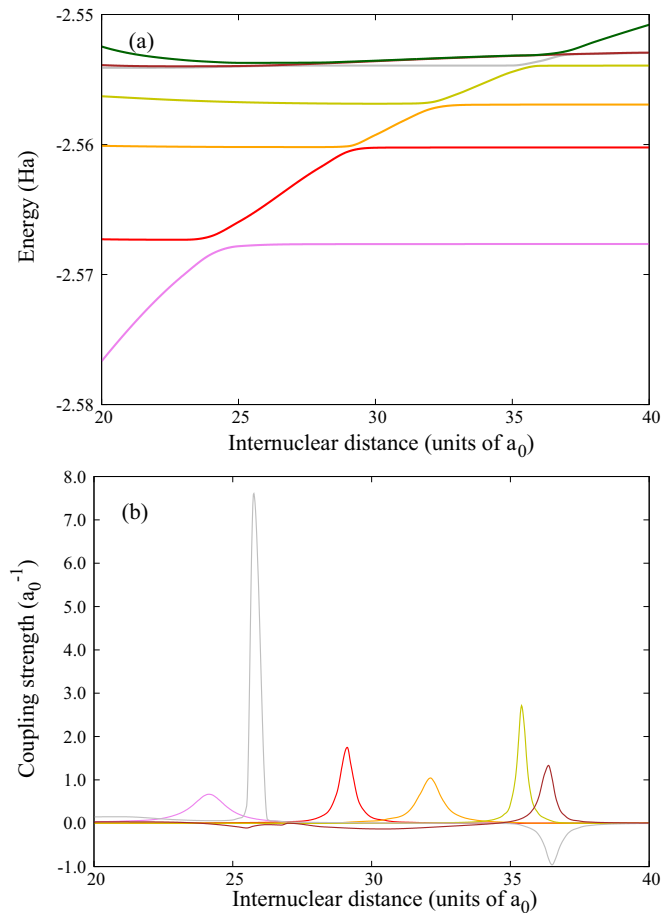


FIG. 5. In (a), the avoided crossings between adiabatic potential energy curves of $^2\Sigma^+$ symmetry originating from the interactions between the ion-pair state and covalent states associated with the $\text{He}[(1s)^1(3l)^2] + \text{H}$ limits are displayed. In (b) the corresponding nonadiabatic coupling elements (between neighboring states) are shown.

distances smaller than $5a_0$, there are large nonadiabatic coupling elements due to avoided crossings among the resonant states that are Rydberg states converging to different excited ionic cores. This is the region where autoionization widths

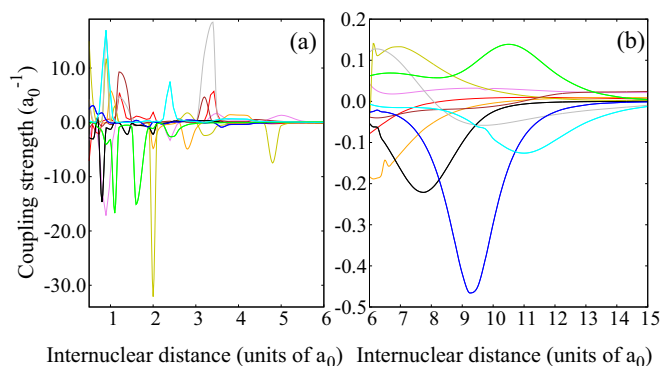


FIG. 6. Nonadiabatic first derivative coupling elements between neighboring HeH electronic resonant states of $^2\Sigma^+$ symmetry at (a) small and (b) intermediate internuclear distances.

are nonzero. The resonant states are therefore interacting with the ionization continuum. The approach to compute the nonadiabatic coupling elements using standard structure calculations and identifying the resonant states by analyzing the configurations of the wave function is approximate. However, as will be shown, for the mutual neutralization reaction the exact magnitudes of the nonadiabatic coupling elements at small internuclear distances ($<5a_0$) are not significant. The avoided crossing due to interactions between the ion-pair state and the $n = 2$ covalent states occurring around $6\text{--}15a_0$ are not as sharp and hence the corresponding coupling elements [see Fig. 6(b)] are smaller than the $n = 3$ coupling elements.

The nonadiabatic coupling elements are computed both analytically at the MRCI level as well as using the finite difference method using the FCI wave functions. At large internuclear distances, the two methods provide identical coupling elements, while at small distances they are similar in form and magnitude.

B. Total cross section and isotope effects

The total mutual neutralization cross section is calculated for collision energies ranging between 1 meV and 300 eV. In Fig. 7, the $^4\text{He}^+ + \text{H}^-$ and $^4\text{He}^+ + \text{D}^-$ cross sections are compared with measured ones [18,21,22] and previous theoretical predictions [23,24]. At large energies, the cross sections connect smoothly to the measured and previous calculated ones. However, at lower energies the calculated cross section is larger than the one measured using a merged-beam apparatus by Peart and Hayton [21]. The measured cross section does not display the same low-energy E^{-1} behavior as observed from the calculation and which is predicted by Wigner's threshold law [39].

The role of autoionization can be investigated by turning on and off the imaginary term W_{ij} as described by Eqs. (2) and (3). In Fig. 8, the total mutual neutralization cross section in collisions of $^4\text{He}^+$ and H^- is displayed both when autoionization is included and when it is not considered. As can be seen, the effect of autoionization is negligible. This is

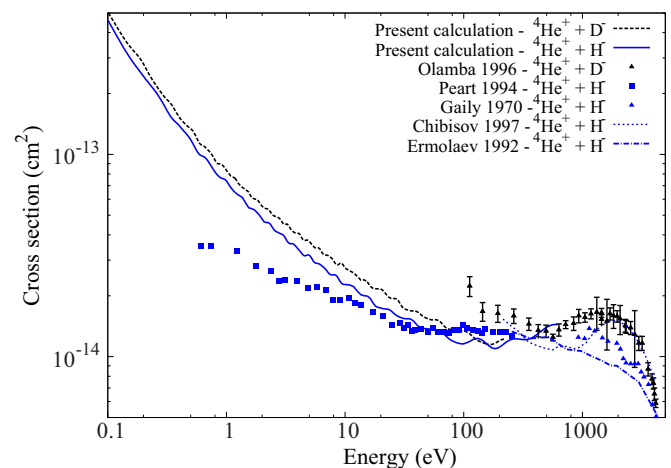


FIG. 7. Calculated cross section of mutual neutralization in collisions of $^4\text{He}^+ + \text{H}^-$ and $^4\text{He}^+ + \text{D}^-$ are compared with previous measurements [18,21,22] and theoretical predictions [23,24].

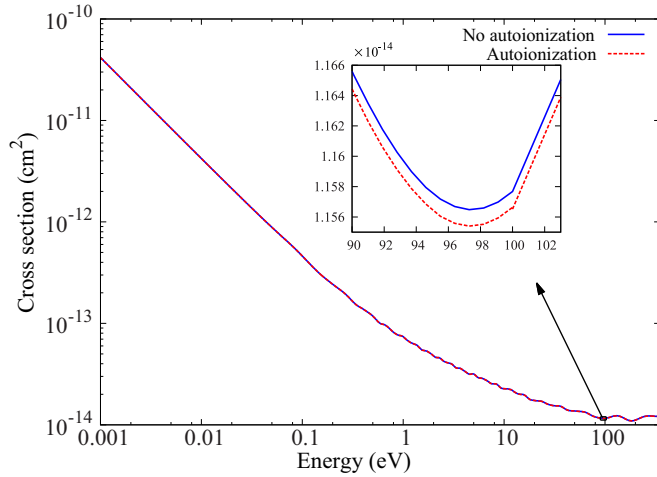


FIG. 8. Calculated cross section of mutual neutralization in collisions of ${}^4\text{He}^+ + \text{H}^-$ with and without inclusion of autoionization.

due to the fact that the autoionization widths are nonzero only at small internuclear distances ($R \leq 5a_0$). At low energies, the centrifugal barrier which is added to the potentials, will prevent the system from reaching these small distances.

The cross sections for mutual neutralization have been calculated for collisions of different isotopes of the hydrogen and helium ions. For the different isotopologues, we assume the adiabatic potential-energy curves and nonadiabatic coupling elements are the same, but the reduced mass of the molecular system is changed. In Fig. 9, we compare the calculated cross sections for collisions of ${}^3\text{He}^+$ or ${}^4\text{He}^+$ with H^- or D^- . The cross sections for the heavier isotopologues have a smaller magnitude than the lighter ones. At large collision energies ($E > 200$ eV), the orders of the cross sections are reversed. A similar isotope effect was found in mutual neutralization in collisions of H^+ with H^- [14]. When the charge-transfer reaction is driven by nonadiabatic couplings occurring at large internuclear distances, the isotope effect will be relatively small. This is the case for both the $\text{He}^+ + \text{H}^-$ and the $\text{H}^+ + \text{H}^-$ mutual neutralization reactions. However,

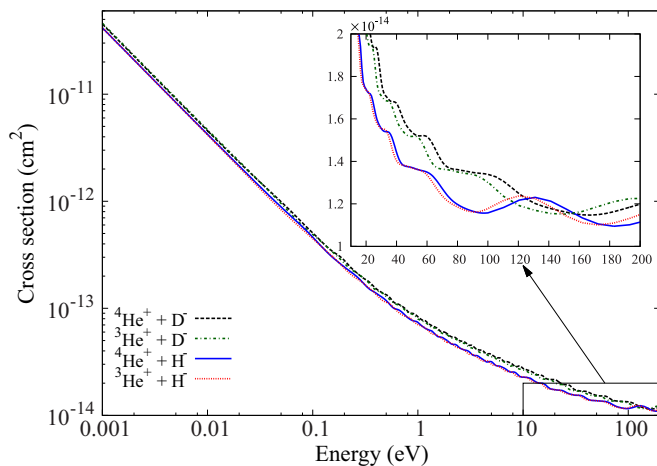


FIG. 9. Calculated cross section of mutual neutralization in collisions of different isotopes of hydrogen and helium ions.

when the reaction is driven by couplings occurring at smaller internuclear distances, the isotope effect can be significant. This was observed in collisions of H^+ (or D^+) with F^- [11]. A similar conclusion is obtained from studies of charge transfer in collisions of He^{2+} with H . At low collision energies, where the reaction is driven by rotational couplings acting at small distances, the isotope effect can be strong [40].

As described in Sec. III A, there are very large nonadiabatic couplings among the resonant states at small internuclear distances. This is the region where autoionization widths are nonzero and our approach to compute the coupling elements using structure methods is approximate. We investigate the effects of these nonadiabatic couplings at small distances by running calculations on the mutual neutralization reaction when all coupling elements smoothly are turned to zero for distances smaller than $5.0a_0$. At low energies, the calculated total cross section will then decrease by a few percent (1%–5% for $E < 10$ eV), while at energies larger than 100 eV, the reduction increases to 18%. Thus the nonadiabatic couplings at small internuclear distances have no significant effect on the mutual neutralization cross section.

Previous quantum mechanical studies on mutual neutralization reactions have neglected rotational couplings [6–13]. However, in the review on recombination processes written in 1982, Bardsley pointed out that rotational couplings could be important in mutual neutralization reactions and should be considered [41]. The rotational couplings originate from correlation between the rotational motion of the nuclei and the electronic motions and it will give rise to different diagonal and off-diagonal terms that should be added to the Hamiltonian. The L -uncoupling terms will induce interactions between the resonant states of ${}^2\Sigma^+$ and ${}^2\Pi$ symmetry that approximately have the form [42]

$$-\frac{\sqrt{\ell(\ell+1)}}{2\mu R^2} \langle \Phi_{\Pi}^i | L_+ | \Phi_{\Sigma}^j \rangle. \quad (9)$$

Due to the factor R^{-2} , these rotational couplings are localized at small internuclear distances. However, the factor $\sqrt{\ell(\ell+1)}$

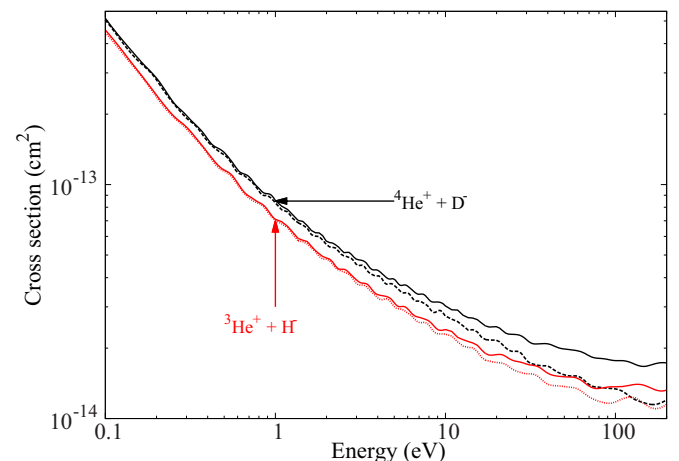


FIG. 10. Calculated cross sections of mutual neutralization in ${}^3\text{He}^+ + \text{H}^-$ and ${}^4\text{He}^+ + \text{D}^-$ collisions with (dotted-dashed lines) and without (solid lines) the inclusion of rotational couplings between ${}^+\Sigma^+$ and ${}^2\Pi$ resonant states.

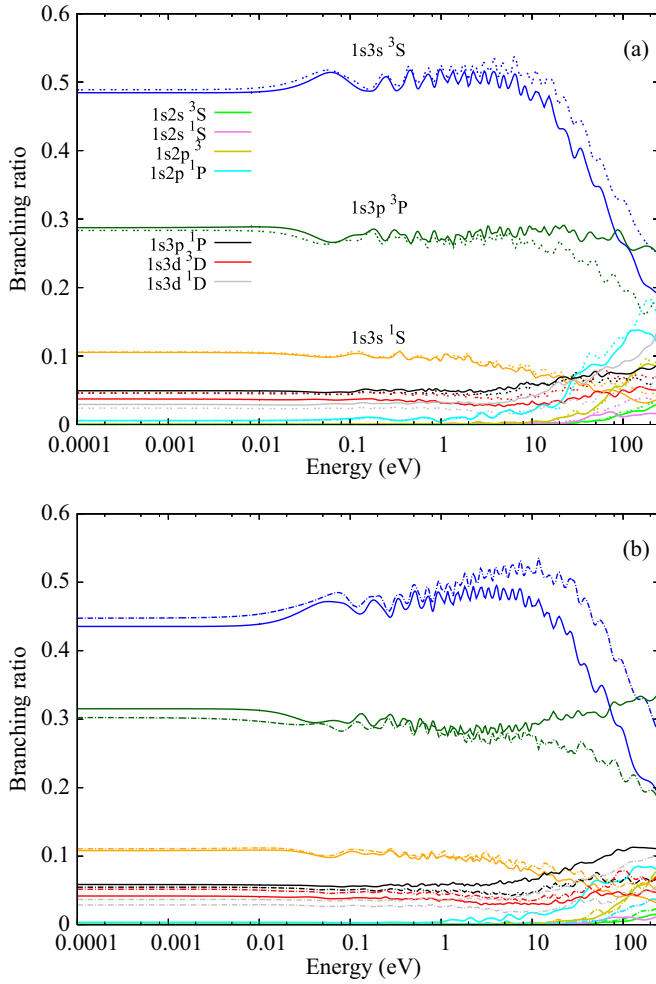


FIG. 11. Calculated final-state distributions in mutual neutralization in (a) ${}^4\text{He}^+ + \text{H}^-$ and (b) ${}^4\text{He}^+ + \text{D}^-$ collisions with (dashed lines) and without (solid lines) inclusion of rotational couplings.

will make the rotational couplings large when high angular momenta quantum numbers contribute. This is the case in the mutual neutralization reaction presently studied. The rotational couplings are not calculated *ab initio*, but are here approximated using a pure precession approximation. The dominant configurations of the adiabatic states have been identified and for the ${}^2\Sigma^+$ and ${}^2\Pi$ states associated with the same asymptotic limit they only differ by the highest occupied molecular orbital and we have

$$\langle \Phi_{\Pi}^i | L_+ | \Phi_{\Sigma}^j \rangle \approx \langle (n\rho\pi)^i | l_+ | (n\rho\sigma)^j \rangle \approx \sqrt{2}. \quad (10)$$

For ${}^2\Sigma^+$ and ${}^2\Pi$ states not associated with the same asymptotic limits, the rotational couplings are approximated with zero. In the diabaticization procedure, the rotational couplings are transformed with a transformation matrix of block-diagonal form

$$\tilde{\mathbf{T}} = \begin{pmatrix} \mathbf{T} & \mathbf{0} \\ \mathbf{0} & \mathbf{1} \end{pmatrix}, \quad (11)$$

where \mathbf{T} is the orthogonal transformation matrix for the ${}^2\Sigma^+$ resonant states computed by numerically solving Eq. (4) above

and $\mathbf{1}$ is a 6×6 unit matrix. No nonadiabatic interactions among the ${}^2\Pi$ states are considered.

The total mutual neutralization cross sections are calculated for collisions of all isotopes of hydrogen and helium ions, with and without the inclusion of the rotational couplings as displayed in Fig. 10 with dotted-dashed and solid lines, respectively. The cross sections are shown for the ${}^3\text{He}^+ + \text{H}^-$ and ${}^4\text{He}^+ + \text{D}^-$ collisions, which are the isotopologues where the rotational couplings have the largest and smallest effects. As can be seen, the rotational couplings will at large collision energies ($E > 10$ eV) increase the neutralization cross section. The effect is largest for the system where the most partial waves contribute.

C. Final-state distributions

From the scattering matrix elements, not only the total cross section can be computed, but also the final-state distributions. Figure 11 shows calculated branching ratios for collisions of ${}^4\text{He}^+ + \text{H}^-$ in (a) and ${}^4\text{He}^+ + \text{D}^-$ in (b) both with (dashed lines) and without (solid lines) the inclusion of rotational couplings.

The dominant channels are all associated with the $\text{He}[(1s)^1(3l)^1] + \text{H}$ limits and these are the covalent states with avoided crossings due to interactions with the ion-pair state at internuclear distances ranging from 20 to $40a_0$ as displayed in Fig. 4. Most important is the state associated with the $1s3s \ 3S$ limit, which has the lowest potential-energy curve of the $n = 3$ states shown in Fig. 5(a). Note that although the isotope effect in the total cross section is very small, there is some isotope dependence in the final-state distributions.

D. Differential cross section

The differential cross section is calculated from the scattering amplitude as described by Eq. (8). In Fig. 12, the total differential cross section (summed over all channels) is displayed for selected collision energies for collisions of ${}^4\text{He}^+$ with H^- . As can be seen, the differential cross section is peaked at small scattering angles (forward direction), with fast oscillations that at a given scattering angle become

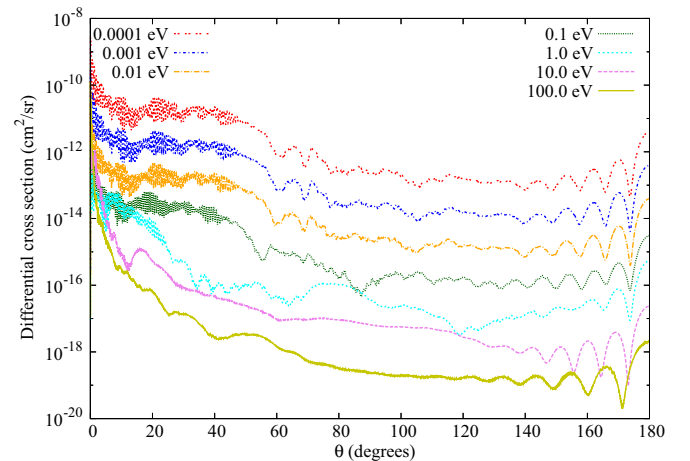


FIG. 12. Differential cross section for mutual neutralization in collisions of ${}^4\text{He}^+$ and H^- at selected collision energies.

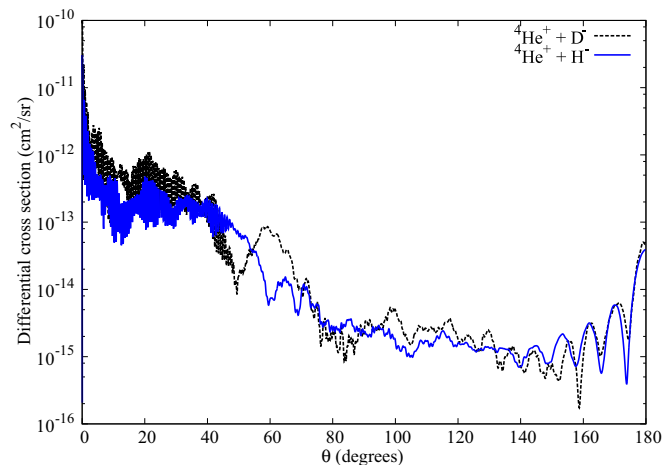


FIG. 13. Differential cross section for mutual neutralization in collisions of ${}^4\text{He}^+ + \text{H}^-$ and ${}^4\text{He}^+ + \text{D}^-$ at 0.1 collision energy.

slower. Similar shapes of differential cross sections have been observed in mutual neutralization reactions between other heteronuclear atomic ions such as $\text{Li}^+ + \text{H}^-$ [8] and $\text{Li}^+ + \text{F}^-$ [13]. It has been discussed [8,43] that this transition between slow and fast oscillations reflects the Coulomb scattering angle where the transition takes place at the distance of closest approach and when the collision energy increases, the transition angle decreases.

The differential cross sections are computed for collisions of the different isotopes of the helium and hydrogen ions. They all show similar behavior of differential cross sections, although the exact positions of the oscillations may vary. As an example, the differential cross sections for mutual

neutralization in collisions of ${}^4\text{He}^+ + \text{H}^-$ and ${}^4\text{He}^+ + \text{D}^-$ at 0.1 eV collision energy are displayed in Fig. 13.

IV. CONCLUSION

Mutual neutralization in collisions of He^+ and H^- is studied *ab initio*, where the nuclear motion is described quantum mechanically. The reaction involves electronic resonant states of HeH of ${}^2\Sigma^+$ symmetry that have been computed by combining electron-scattering calculations with structure calculations at the FCI and MRCI level of theory. Nonadiabatic couplings are computed analytically. Total and differential cross sections are calculated as well as final-state distributions. The reaction is studied for collisions of various isotopes of hydrogen and helium ions. The total cross section is in agreement with measurements and previous theoretical studies at higher energies, but is larger than the cross section measured using a merged beam apparatus [21] at relatively low energies. At low collision energies, the autoionization and the rotational couplings between the ${}^2\Sigma^+$ and ${}^2\Pi$ states, estimated using a pure precession approximation, are found to have a small effect on the outcome of the reaction. The mutual neutralization reaction will be dominated by formation of $\text{He}[1s3s\ ^3S] + \text{H}$ followed by $\text{He}[1s3p\ ^3P] + \text{H}$ with ratios of approximately 50% and 30%, respectively, at low collision energies. The calculated differential cross section is peaked in the forward direction.

ACKNOWLEDGMENTS

We acknowledge support from the Swedish research council (VR) (Grant No. 2014-4164) and A.E.O. acknowledges support from the National Science Foundation under Grant No. PHY-11-60611.

-
- [1] D. R. Bates and J. T. Lewis, *Proc. Phys. Soc. A* **68**, 173 (1955).
 [2] R. E. Olson, J. R. Peterson, and J. Moseley, *J. Chem. Phys.* **53**, 3391 (1970).
 [3] H. M. Hedberg, S. Nkambule, and Å. Larson, *J. Phys. B: At., Mol., Opt. Phys.* **47**, 225206 (2014).
 [4] L. Landau, *Phys. Z. Sowjetunion* **2**, 46 (1932).
 [5] C. Zener, *Proc. R. Soc. A* **137**, 696 (1932).
 [6] S. Beinstock and A. Dalgarno, *J. Chem. Phys.* **78**, 224 (1983).
 [7] D. Fussen and C. Kubach, *J. Phys. B: At., Mol., Opt. Phys.* **19**, L31 (1986).
 [8] H. Croft, A. S. Dickinson, and F. X. Gadea, *J. Phys. B: At., Mol., Opt. Phys.* **32**, 81 (1999).
 [9] A. S. Dickinson, R. Poteau, and F. X. Gadea, *J. Phys. B: At., Mol., Opt. Phys.* **32**, 5451 (1999).
 [10] M. Stenrup, Å. Larson, and N. Elander, *Phys. Rev. A* **79**, 012713 (2009).
 [11] J. Zs. Mezei, J. B. Roos, K. Shilyaeva, N. Elander, and Å. Larson, *Phys. Rev. A* **84**, 012703 (2011).
 [12] A. K. Belyaev, P. S. Barklem, A. Spielfiedel, M. Guitou, N. Feautrier, D. S. Rodionov, and D. V. Vlasov, *Phys. Rev. A* **85**, 032704 (2012).
 [13] S. M. Nkambule, P. Nurzia and Å. Larson, *Chem. Phys.* **462**, 23 (2015).
 [14] S. M. Nkambule, N. Elander, Å. Larson, J. Lecointre, and X. Urbain, *Phys. Rev. A* **93**, 032701 (2016).
 [15] T. N. Rescigno, C. W. McCurdy, A. E. Orel, and B. H. Lengsfeld III, *The Complex Kohn Variational Method*, in *Computational Methods for Electron-molecule Scattering*, edited by W. H. Huo and F. A. Gianturco (Plenum, New York, 1995).
 [16] B. R. Johnson, *J. Comput. Phys.* **13**, 445 (1973).
 [17] B. R. Johnson, *Phys. Rev. A* **32**, 1241 (1985).
 [18] T. D. Gaily and M. F. A. Harrison, *J. Phys. B: At. Mol. Phys.* **3**, 1098 (1970).
 [19] B. Peart, R. Grey, and K. T. Dolder, *J. Phys. B: At. Mol. Phys.* **9**, L373 (1976).
 [20] B. Peart, M. A. Bennett, and K. Dolder, *J. Phys. B: At. Mol. Phys.* **18**, L439 (1985).
 [21] B. Peart and D. A. Hayton, *J. Phys. B: At. Mol. Phys.* **27**, 2551 (1994).
 [22] K. Olamba, S. Szücs, J. P. Chenu, N. El Arbi, and F. Brouillard, *J. Phys. B: At. Mol. Phys.* **29**, 2837 (1996).
 [23] A. M. Ermolaev, *J. Phys. B: At. Mol. Phys.* **25**, 3133 (1992).
 [24] M. Chibisov, F. Brouillard, J. P. Chenu, M. H. Cherkani, D. Fussen, K. Olamba, and S. Szücs, *J. Phys. B: At. Mol. Phys.* **30**, 991 (1997).

- [25] P. Saxe, B. H. Lengsfeld, R. Martin, and M. Page, *MESA (Molecular Electronic Structure Applications)* University of California, 1990.
- [26] D. E. Woon and T. H. Dunning, Jr., *J. Chem. Phys.* **100**, 2975 (1994).
- [27] T. H. Dunning, Jr., *J. Chem. Phys.* **90**, 1007 (1989).
- [28] S. Geltman, *Topics in Atomic Collision Theory* (Academic Press, New York, 1997), p. 31.
- [29] B. H. Lengsfeld and D. R. Yarkony, in *State-Selected and State-To-State Ion-Molecule Reaction Dynamics*, edited by M. Baer and C.-Y. Ng, *Advances in Chemical Physics* Vol. 82 (John Wiley & Sons, Inc., Hoboken, NJ, 1992), Part 2, Chap. 1, pp. 1–71.
- [30] T. F. O'Malley, *Phys. Rev.* **150**, 14 (1966).
- [31] A. U. Hazi, *J. Phys. B: At. Mol. Phys.* **16**, L29 (1983).
- [32] A. E. Orel, *Phys. Rev. A* **62**, 020701 (2000).
- [33] C. W. McCurdy and J. L. Turner, *J. Chem. Phys.* **78**, 6773 (1983).
- [34] J. Royal, Å Larson, and A. E. Orel, *J. Phys. B: At., Mol., Opt. Phys.* **37**, 3075 (2004).
- [35] C. A. Maed and D. G. Truhlar, *J. Chem. Phys.* **77**, 6090 (1982).
- [36] D. E. Manolopoulos, M. J. Jamieson, and A. D. Pradhan, *J. Comput. Phys.* **105**, 169 (1993).
- [37] V. Venturi, I. B. Whittingham, P. J. Leo, and G. Peach, *Phys. Rev. A* **60**, 4635 (1999).
- [38] M. W. Müller, A. Merz, M.-W. Ruf, H. Hotop, W. Meyer, and M. Movre, *Z. Phys. D* **21**, 89 (1991).
- [39] E. P. Wigner, *Phys. Rev.* **73**, 1002 (1948).
- [40] N. Stolterfoht, R. Cabrera-Trujillo, Y. Öhrn, E. Deumens, R. Hoekstra, and J. R. Sabin, *Phys. Rev. Lett.* **99**, 103201 (2007).
- [41] J. N. Bardsley, *Recombination Processes in Atomic and Molecular Physics*, in *Atomic and Molecular Collision Theory*, edited by F. A. Gianturco (Plenum Press, New York, 1982).
- [42] H. Lefebvre-Brion and R. W. Field, *Perturbations in the Spectra of Diatomic Molecules* (Academic Press, Orlando, FL, 1986).
- [43] G. A. L. Delvigne and J. Los, *Physica* **67**, 166 (1973).